Impact of changing Arctic sea ice extent, sea ice age, and snow depth on sea salt aerosol from blowing snow and the open ocean for 1980-2017

Kaitlyn Confer

A thesis

submitted in partial fulfillment of the

requirements for the degree of

Master of Science

University of Washington

2022

Committee:

Lyatt Jaeglé

Becky Alexander

Ed Blanchard-Wigglesworth

Program Authorized to Offer Degree:

Department of Atmospheric Science

University of Washington

Abstract

Impact of changing Arctic sea ice extent, sea ice age, and snow depth on sea salt aerosol from blowing snow and the open ocean for 1980-2017

Kaitlyn Confer

Chair of the Supervisory Committee:

Lyatt Jaeglé

Department of Atmospheric Sciences

The Arctic is undergoing rapid change: temperature is rising at double the rate as the global average, sea ice extent is declining, the age of sea ice is becoming younger, and snow depth on sea ice is thinning. The effect of these changes on sea salt aerosol (SSA) produced by oceanic wave-breaking and the sublimation of wind-lofted salty blowing snow on sea ice is poorly understood. We use the GEOS-Chem chemical transport model to quantify how Arctic SSA concentrations have changed and assess the relative roles of changing extent of the open ocean, multi-year sea ice (MYI), first-year sea ice (FYI), and snow depths on SSA emissions for 1980-2017. We combine snow depths from the Lagrangian snow-evolution model (SnowModel-LG) together with an empirically-derived snow salinity function of snow depth to derive spatially and temporally varying surface snow salinity over Arctic FYI. We implement this surface snow salinity in the GEOS-Chem model, which simulates SSA emissions from blowing snow and from the open ocean. We contrast this simulation of SSA with a GEOS-Chem simulation assuming

uniform snow salinity on FYI. Both simulations are consistent with multiyear (2005–2014) in situ observations of SSA mass concentrations at four sites in the Arctic. We find that surface snow salinity on Arctic sea ice is increasing at a rate of ~30% decade^{-1} and SSA emissions are increasing at a rate of 7-9% decade^{-1} during the cold season (November-April). These increases are due to the replacement of MYI with more saline FYI and thinning snow depth on sea ice. As a result, simulated SSA mass concentrations over the Arctic increase by 8-12% decade^{-1} in the cold season for the 1980-2017 period. This is consistent with the observed 10-12%/decade trend in SSA mass concentrations at Alert, Canada. During the warm season (May-Oct), our simulation predicts that SSA mass concentrations over the Arctic increase by 7-11% decade^{-1}. This warm season increase is due to decreasing sea extent which results in increasing open ocean emissions of SSA. These large changes in SSA concentrations could potentially affect past and future bromine explosions as well as Arctic climate feedbacks.

1 Introduction.

Breaking waves over the open ocean are recognized as the main mechanism for the global production of SSA (de Leeuw et al., 2011; Lewis & Schwartz, 2004, and references therein). In polar regions, sea ice and snow-sourced SSA have been proposed as significant regional sources of SSA via the sublimation of wind-lofted salty blowing snow on sea ice (Simpson et al., 2007; Yang et al., 2008) and highly saline frost flowers (Domine et al., 2004; Kaleschke et al., 2004; Rankin et al., 2002). However, the role of frost flowers as a direct source of SSA is uncertain as several field and laboratory experiments have demonstrated that frost flowers are difficult to break even under strong wind conditions (Alvarez-Aviles et al., 2008; Roscoe et al., 2011; Yang et al., 2017). Recent modeling efforts have been most successful in reproducing the seasonal cycle of SSA mass concentrations observed at multiple polar sites with a blowing snow source and have found that blowing snow is the dominant source of SSA in polar regions during winter and spring (Huang & Jaeglé, 2017; Rhodes et al., 2017). Several studies have proposed that snow-sourced SSA likely plays an important role in polar tropospheric ozone and halogen chemistry through the release of active bromine in polar spring contributing to ozone depletion events (ODEs) (Choi et al., 2018; Huang et al., 2020; Kalnajs et al., 2013; Marelle et al., 2021; Swanson et al., 2022; Yang et al., 2010).

The cold season polar emissions of SSA from blowing snow are strongly influenced by meteorological factors (wind speed, temperature, relative humidity) as well as sea ice properties, such as extent, age, and snow depth (Frey et al., 2019; Yang et al., 2008). When sea ice retreats during summer and fall, open ocean SSA emissions dominate and are influenced by sea ice extent as well as wind speed and sea surface temperatures (Struthers et al., 2011). Therefore,

there is potential for a significant perturbation of Arctic SSA concentration and composition in response to the large changes in Arctic climate and sea ice properties that have occurred over the past decades (Abbatt et al., 2019; Schmale et al., 2021) and are expected to continue in the coming decades (Fox-Kemper et al., 2021). A quantitative understanding of such changes in SSA is critical since SSA influences radiative forcing and therefore climate both directly by absorbing and scattering sunlight and indirectly by modifying the reflectivity, emissivity, lifetime, and extent of clouds (DeMott et al., 2016; O'Dowd et al., 1997; Struthers et al., 2011).

Is there any evidence for changing SSA mass concentrations over the Arctic? Long-term observations at high northern latitude sites are scarce and have provided contradicting results so far. Sharma et al. (2019) found that at Alert, Nunavut, Canada sea salt derived Na^+ and Cl^- increased by 19% and 43%, respectively, between 1980 and 2013 during the winter (January-March). These increases were based on the change in the long-term trend factor for the first 5 years relative to the last 5 years and were significant at $p<0.01$. Schmale et al. (2022) examined long-term trends of observed Na^+ concentrations at Alert (1980-2017), Barrow (1998-2014), Zeppelin (1992-2019), and Villum (1991-2017) for the haze season (January-April) and the summer season (June- September) using the seasonal median values. They found no statistically significant trends at any of these sites.

Most of the previous modeling work on aerosol climatic effects in the Arctic has focused on long-range transported anthropogenic pollution (Arctic haze), with relatively little emphasis on natural aerosol sources, which remain highly uncertain (e.g. Schmale et al., 2021and references therein). In particular, several modeling studies have examined the effect of retreating sea ice on

the open ocean source of SSA during summer (Browse et al., 2014; Gilgen et al., 2018; Struthers et al., 2011). They predicted that open ocean SSA emissions increased by factors 1.7-10 relative to present day, with the magnitude of the increase depending on the magnitude of sea ice extent decrease in the models. The resulting climate impact ranged from little to no effect (Browse et al., 2014), as a result of suppression of nucleation, to a significant negative feedback on climate, with more negative direct and indirect radiative forcing (Gilgen et al., 2018; Struthers et al., 2011). To our knowledge, the impact of changing cold season Arctic conditions on SSA emissions from blowing snow has not been examined.

One of the key parameters in controlling the magnitude of blowing snow SSA emissions is the surface snow salinity. Snow salinity itself is influenced by sea ice age and snow depth (Domine et al., 2004), which have both been decreasing over the last few decades (e.g., Kwok, 2018; Webster et al., 2014). Brines are often present at the sea ice–snow interface and can travel upward through the snow by capillary forces (Perovich & Richter-Menge, 1994). This upward migration from the sea ice surface through the snowpack is the dominant source of salinity for thin snow over sea ice (< 17 cm) (Massom et al., 2001; Peterson et al., 2019). Other sources of snow salinity include frost flower formation, atmospheric deposition of SSA, and sea water flooding caused by snow accumulation (Yang et al., 2008).

The salt migration distance from the sea ice surface through the snowpack has a strong influence on the salinity of surface snow, with thinner snow depths leading to higher salinities (Domine et al., 2004; Frey et al., 2019; Massom et al., 2001). In a snowpack with a mean depth of 16 cm, low salinities (< 0.1 psu) are observed in the top 4 cm, below which salinity increases to ~1 psu at 7 cm above the ice surface and increases further to ~2 psu at 2 cm above the ice surface

(Nandan et al., 2017). With increasing snow depth, the salinity of surface snow decreases, and the influence of atmospheric deposition can become more important (Krnavek et al., 2012; Nandan et al., 2017). While deposition typically results in lower values of salinity (0.01-0.1 psu), these lower salinities have more than enough sea salt to account for observed increases in atmospheric SSA during storms if released by sublimation (Frey et al., 2019). Snow over first year ice (FYI) will generally be more saline than over older multi-year ice (MYI) as MYI is desalinated by brine drainage during summer melt cycles (Cox & Weeks, 1974). Thus, over MYI, atmospheric deposition of SSA is likely the main source of surface snow salinity (Peterson et al., 2019). Previous modeling of blowing snow SSA emissions assumed spatially and temporally uniform snow salinity on FYI and MYI (Frey et al., 2019; Huang et al., 2018, 2020; Huang & Jaeglé, 2017; Rhodes et al., 2017; Yang et al., 2008, 2010, 2019). In this study, we derive an empirical snow depth-salinity dependence based on snow salinity observations. We combine this empirical relationship with snow depth calculated from the Lagrangian snow-evolution model (SnowModel-LG) to infer spatially and temporally varying surface snow salinity. We conduct a SSA simulation over a 38-year period (1980-2017) in order to understand the impact of decreasing sea ice extent, sea ice age, and snow depths on the distribution of SSA mass concentrations throughout the Arctic. The models and observations used in this study are described in Section 2. In section 3, we examine the response of surface snow salinity to changing Arctic sea ice extent, age, and snow depth. The resulting evolution of SSA emissions and mass concentrations are discussed in Section 4. We compare modeled trends in SSA mass concentrations to observations at Alert, Canada in Section 5. Conclusions are presented in Section 6.

2 Models and observations

2.1 GEOS-Chem chemical transport model

We use the GEOS-Chem (v13.0.2) 3-D global chemical transport model (Bey et al., 2001) driven by the Modern-Era Retrospective analysis for Research and Applications, version 2 (MERRA-2) assimilated meteorological fields (Gelaro et al., 2017), which have a native horizontal resolution of 0.5º latitude by 0.625º longitude with 72 vertical levels. SSA emissions are calculated at this native horizontal resolution using the Harmonized Emission Component (HEMCO) (Keller et al., 2014). For computational expediency, we regrid the HEMCO SSA emissions and MERRA-2 meteorological fields to a 2º x 2.5º horizontal resolution and 47 vertical levels with merged levels above 80 hPa to conduct the SSA simulations within GEOS-Chem.

The open-ocean emissions of SSA in GEOS-Chem are a function of wind speed and sea surface temperature (SST) as described in Jaeglé et al. (2011). Huang and Jaeglé (2017) implemented blowing snow SSA emissions in GEOS-Chem based on the parameterization of Yang et al. (2008, 2010). The SSA production from blowing snow is a function of relative humidity, temperature, age of snow, snow salinity, and wind speed. The Yang et al. (2008, 2010) parameterization was originally based on blowing-snow measurements above ice sheets (Budd, 2013; Mann et al., 2000; Nishimura & Nemoto, 2005) and the Canadian Prairies (Déry & Yau, 1999, and references therein) but have since been validated against direct observations of SSA production from blowing snow above sea ice (Frey et al., 2019). The minimum wind speed needed to saltate and suspend snow particles from the sea ice surface is temperature dependent. The size distribution of suspended blowing snow particles follows a two-parameter gamma distribution (Yang et al., 2008, and references therein). As in Huang and Jaeglé (2017), we assume a mean snow age of 3 days for the Arctic.

In our previous work (Huang et al., 2018, Huang et al., 2020), we assumed a uniform salinity of 0.1 psu for snow on FYI and 0.01-0.05 psu for snow on MYI in the Arctic. The MERRA-2 boundary conditions for sea ice concentrations are described in Gelaro et al. (2017) and are derived from the monthly 1° product from Taylor et al. (2000) prior to 1982, the daily 1/4° product from Reynolds et al. (2007) for 1982 until March 2006, and the daily 1/20° product from Donlon et al. (2012) after March 2006. In our previous work, we inferred the location of MYI sea ice based on the preceding summertime minimum sea ice extent from MERRA-2. The location of MYI was then assumed to be invariant until the next summer. We have updated this approach to instead use the EASE-Grid Sea Ice Age, Version 4 product distributed at the National Snow & Ice Data Center (NSIDC, (M. Tschudi et al., 2019). This dataset provides weekly Arctic sea ice age since January 1984 and is described in Tschudi et al. (2020). For years prior to 1984, we assign MYI extent based on the minimum sea ice extent from MERRA-2 at the end of summer of the previous year.

Dry deposition of SSA over land accounting for particles growth under high humidity conditions follows the size-segregated scheme described in Zhang et al. (2001). The dry deposition velocity over the ocean is calculated based on the Slinn and Slinn (1980) deposition model for natural waters. Over snow and ice surfaces, Fisher et al., 2011 implemented a dry deposition velocity of 0.03 cm s^{-1} based on the measurements of Nilsson et al. (2001). The wet deposition scheme includes convective updraft scavenging, rainout, and washout from precipitation (Liu et al., 2001), and snow scavenging (Wang et al., 2011). For this work, we track SSA mass in two size bins, accumulation mode (r_{dry} = 0.01–0.5 μm) and coarse mode (r_{dry} = 0.5–8 μm), except in the comparison to in situ mass concentrations of SSA for which we use r_{dry} = 0.01–0.3 μm and r_{dry} = 0.3–3 μm similar to Huang and Jaeglé (2017). In the rest of the paper, we will refer to the

accumulation and coarse-mode SSA as submicron and supermicron SSA based on their diameters.

2.2 SnowModel-LG

SnowModel-LG is a prognostic lagrangian ice-parcel tracking snow model that includes physical snow processes including rainfall, snowfall, sublimation from static surfaces and blowing snow, blowing snow redistribution, snow density evolution, and snowpack metamorphosis (Liston et al., 2020). Within the lagrangian framework, the model redistributes snow around the Arctic basin as the sea ice moves and is the only data product that includes snow depth during the melt season (Zhou et al., 2021). The model is forced by precipitation, 2m air temperature, wind speed and direction from two reanalysis products (MERRA-2 and ERA5) and by weekly ice motion vectors from NSIDC (M. Tschudi et al., 2019; M. A. Tschudi et al., 2020).

SnowModel-LG was used to produced daily, pan-Arctic, snow depth distribution on a 25x25 km grid from August 1980 through July 2018 (Liston et al., 2020). Stroeve et al. (2020) evaluated SnowModel-LG against several data sets including Operation IceBridge, ice mass balance buoys, MagnaProbes and passive microwave estimates. They found that the model captured observed spatial and seasonal variability in snow depth accumulation, while also showing statistically significant declines in snow depth since 1980 during the cold season. For application in our study, we use SnowModel-LG forced by MERRA-2 and regrid the SnowModel-LG daily snow depth to the native MERRA-2 resolution.

2.3 Implementation of snow depth-dependent surface snow salinity

We use in situ observations of snow salinity on Arctic sea ice reported in four different studies (Ewert et al., 2013; Krnavek et al., 2012; Nandan et al., 2017; Peterson et al., 2019). More than half of the samples used in our work were collected during nine field campaigns in the Canadian Arctic (see Fig. 1a) as summarized in Nandan et al. (2017). These samples were taken in April-May between 2004 and 2017, on both undeformed and slightly deformed FYI. More samples of snow were collected from landfast FYI near Utqiaġvik/Barrow, AK, during February 2010 and March 2011 in the Ewert et al. (2013) study. Krnavek et al. (2012) collected surface snow samples during March and April over three years (2004, 2005, and 2007) from the frozen Arctic Ocean for thin and thick FYI, as well as over MYI. Lastly, Peterson et al. (2019) collected snow samples over both FYI and MYI in regions across the Arctic Ocean accessed via aircraft in April-May 2013, February 2014, and April 2014.

Figure 1b shows all 1440 individual in situ salinity observations as a function of snow depth above the sea ice surface. We only show observations collected over FYI. Very high salinity values occur within the first 4 cm above the sea ice surface, often exceeding 5 psu and reaching up to 35 psu, and then salinity rapidly decrease with increasing snow depth until 20 cm depth. This overall behavior is consistent with upward migration of brine from the sea ice surface up 20 cm (Domine et al., 2004). Above 20 cm salinities tend to be much lower, typically <0.05 psu, but sometimes reaching higher values. We hypothesize that the likely origin of the salinity above 20 cm is from atmospheric deposition of SSA.

We separate the salinity observations in 10 snow depth bins and calculate the median salinity for each bin: 0-2 cm (11.9 psu, n=239 observations), 2-4 cm (7.1 psu, n=220), 4-6 cm (2.8 psu, n=222), 6-8 cm (1.5 psu, n=148), 8-10 cm (1.27 psu, n=104),10-12 cm (1 psu, n=88), 12-15 cm

(0.2 psu, n=129), 15-20 cm (0.057 psu, n=65), 20-25 cm (0.036 psu, n=51), 25 cm and above (0.035 psu, n=35). The top two bins representing observations >20 cm have similar medians ~0.035 psu and we use this value as our minimum salinity for all sea ice ages. For the bins below 20 cm, we fit the median salinities with an exponential function of snow depth (z is snow depth in cm): salinity=16.47 exp(-0.312 z).

We combine this empirical exponential function with daily snow depths from SnowModel-LG (Section 2.2) to calculate surface snow salinity. This expression leads to very high salinities for thin snow cover, which generally occurs over newly formed sea ice in the Fall. Observations show that the surface of young sea ice is covered by a thin, highly saline layer of slush, thus the snow itself is highly saline but also contains large amounts of liquid (Drinkwater & Crocker, 1988; Langlois & Barber, 2007). This slushy brine-wetted snow is unlikely to be lifted by winds. To account for this, we implement a snow-holding depth, which is the snow depth that must be exceeded before snow becomes available for wind transport (Liston & Sturm, 2002). We conducted sensitivity studies varying the snow-holding depth between 2 and 10 cm and evaluated our results against observations of SSA mass concentrations (section 2.5). Based on these sensitivity studies, we found that a snow-holding depth of 8 cm is most consistent with observations. We thus use this 8 cm snow-holding depth to calculate blowing snow SSA emissions. We apply the following equation to derive spatially and temporally varying snow salinity over sea ice:

$$\begin{cases} salinity_{FYI} = 16.47 exp(-0.312\ z)\ psu, 8 < z < 20 cm \\ salinity_{FYI} = 0.035 \text{ psu}, \quad z \geq 20 \text{ cm} \\ salinity_{MYI} = 0.035\ psu \end{cases} \qquad \text{Equation 1}$$

where z is snow depth in cm. Figure 2b shows the spatial distribution of surface snow salinities calculated by applying Equation 1 to SnowModel-LG's snow depths (Fig. 2a) for February-April 2005-2014. The highest salinities (0.1-1.35 psu) occur over FYI in regions with very thin snow depths (<15 cm) located mainly in the Kara, Chukchi, and Laptev Seas. Figure 2c shows the mean salinity assumed fixed salinities of 0.1 psu over FYI and 0.035 psu over MYI. Using the varying salinity model, the mean salinity over FYI is 0.18 psu, nearly double the mean of FYI fixed salinity. Compared to the blowing snow SSA emissions with fixed salinity (Fig. 2e), the blowing snow SSA emissions with the variable salinity (Fig. 2d) are enhanced in the Eastern Arctic (Kara, Chukchi, and Laptev Seas) where snow depths are thinnest.

2.4 Simulations conducted as part of this work

We conduct four GEOS-Chem aerosol simulations for 1980-2017 : (1) a baseline simulation (referred to as "OO"), in which the only source of SSA is from the open ocean; (2) a simulation that includes open ocean and blowing snow SSA sources on MYI (referred to as "OO+MYI"), where only MYI is a source of blowing snow, assuming a fixed salinity of 0.035 psu; (3) a simulation that includes open ocean and blowing snow SSA sources on both FYI and MYI (referred to as "OO+MYI+FYI"), for which we assume fixed surface snow salinity of 0.1 psu on FYI and 0.035 psu on MYI; (4) a simulation with open ocean and blowing snow SSA sources assuming spatially and temporally variable salinity on FYI (section 2.3) and fixed salinity (0.035 psu) on MYI ("OO+MYI+varFYI"). Together, these simulations allow us to separate the individual impact of SSA emissions from the open ocean, MYI (by difference between "OO+MYI" and "OO"), FYI with fixed salinity (difference between "OO+MYI+FYI" and "OO+MYI"), and FYI with variable salinity ("OO+MYI+varFYI" minus and "OO+MYI").

The simulations use the same assumptions for the blowing snow parameterization as in our previous work (section 2.1), apart from surface snow salinity and the number of particles produced per snowflake (N). The value of N influences the size distribution SSA produced from blowing snow but does not change the total emissions. For the OO+MYI+FYI and OO+MYI simulations, we use N=5 as in Huang & Jaeglé (2017). This choice was based on comparisons to wintertime observations of submicron and supermicron SSA at Utqiaġvik/Barrow. The OO+MYI+varFYI simulation results in higher mean salinities and thus a shift of blowing snow SSA to larger sizes. In order to reproduce the wintertime observations of submicron and supermicron SSA at Barrow, we increase N to a value of 10 for that simulation.

Table 1 summarizes the annual mean budgets for individual SSA sources as calculated in GEOS-Chem for 2005-2014 for the region defined in figure 1a. The total (0.01–8 μm) blowing snow source is 0.3 Tg/yr for MYI, 1.5 Tg/yr for MYI+FYI and 2.5 Tg/yr for MYI+varFYI. The larger blowing snow source for the variable salinity are due to the higher salinity values (Fig. 2b). The salinity also affects the size distribution of the blowing snow SSA emissions, with larger SSA at higher salinities (see Equation 7 in Yang et al., 2018). Indeed, the ratio between submicron to supermicron SSA decreases from 1.0 for the MYI simulation (0.035 psu), to 0.75 for the MYI+FYI simulation, and 0.47 for the MYI+varFYI simulation. The smaller ratio for the MYI+varFYI simulation occurs despite the higher number of particles produced from one snowflake (N=10). While the open ocean accounts for most of the emissions and mass concentrations of supermicron SSA (OO: 13.5 Tg/yr and 1.4 $\mu g/m^3$; MYI+FYI: 0.9 Tg/yr and 0.2 $\mu g/m^3$; MYI+varFYI: 1.7 Tg/yr and 0.4 $\mu g/m^3$), submicron SSA are dominated by blowing snow (OO: 0.2 Tg/yr and 0.2 $\mu g/m^3$; MYI+FYI: 0.6 Tg/yr and 0.6 $\mu g/m^3$; MYI+varFYI: 0.8 Tg/yr and 0.8 $\mu g/m^3$).

2.5 Model evaluation with *in situ* observations of SSA mass concentrations at Arctic sites

Figure 3 compares our model simulations to *in situ* observations of SSA mass concentrations at four Arctic sites: Alert, Nunavut, Canada (82.5°N, 62.5°W; 210 m a.s.l.; Sharma et al., 2019); Villum Research Station, Greenland (81.6°N, 16.67°W; Tøseth et al., 2012); Barrow/Utqiaġvik, Alaska, USA (71.3°N, 156.6°W; 11 m a.s.l.; Quinn et al., 2002) and Zeppelin Mountain, Svalbard, Norway (78.9°N, 11.9 °E; 475 m a.s.l.; Tørseth et al., 2012). The location of these sites is indicated in Figure 1a (red stars). To conduct our evaluation, we use observations for 2005–2014, except for Villum, which only has observations starting in 2008. At Barrow/Utqiaġvik Na^+ mass concentrations are available for both submicron and supermicron aerosol, while all the other sites measure total mass concentrations. The aerosol sampling frequency ranges from daily (Zeppelin, submicron at Barrow/Utqiaġvik) to weekly (Alert, Villum). In the winter months, the coastlines near these sites are mostly covered by sea ice. For comparison between the GEOS-Chem model and the observations, we convert observed Na^+ mass concentrations to SSA mass concentrations using a factor of 3.256 based on the mass ratio of Na^+ in seawater (Riley and Chester, 1971).

Observations at all four sites display a similar seasonal cycle, with enhanced SSA mass concentrations (1-1.5 μg m^{-3}) during the cold season (November – April), and lower concentrations (< 0.5 μg m^{-3}) during summer (June-August) (Fig. 3). Zeppelin has a less pronounced seasonal cycle due to its proximity to the North Atlantic ocean.

The OO simulation underestimates the wintertime maximum at Barrow/Utqiaġvik, Alert and Villum by factors of 3-10 but reproduces concentrations during the summer. At Zeppelin, the OO simulations overestimates the observations during the cold season. When a blowing snow source

is added to GEOS-Chem (OO+MYI+FYI and OO+MYI+varFYI), the model can successfully reproduce the seasonal cycle and agreement with observations is improved at Barrow/Utqiaġvik, Alert and Villum. However, at Zeppelin the blowing snow source leads to a larger overestimate of the observations . The higher elevation of Zeppelin results in more influence from the free troposphere and aerosol-cloud interactions (Freud et al., 2017), which together with the complex nearby topography might not be captured by the model. Overall, both blowing snow simulations capture the observed SSA seasonal cycle reasonably well. The addition of temporally and spatially varying salinity on FYI increased the modeled concentrations during the cold season by 0.1-0.3 μg m^{-3}. Note that none of these stations are located close to the high salinity areas (>0.5 psu, Fig. 2b) predicted by our empirical model in the Eastern Arctic, and thus the influence of variable salinity is relatively small at these four sites.

2.6 Trend and significance calculations

We calculate trends using the Theil-San slope from the non-parametric Mann-Kendall test. The test has been widely used with environmental data including Arctic data sets (Collaud Coen, Andrews, Bigi, et al., 2020; Collaud Coen, Andrews, Lastuey, et al., 2020; Heslin-Rees et al., 2020; Skov et al., 2020; Tunved & Ström, 2019). We define a trend to be significant if the p-value is smaller or equal to 0.05. We express the slope in % $decade^{-1}$, relative to the 1980-2017 mean.

These trends are calculated for the means of each season, which we define as Winter (Nov-Jan), Spring (Feb-Apr), Summer (May-Jul) and Fall (Aug-Oct), based on the seasonality of observed SSA mass concentrations in the Arctic (Fig. 3).

3. Response of surface snow salinity to changing Arctic sea ice conditions for 1980-2017

Figure 4a shows the 1980-2017 timeseries of monthly mean sea ice area in the Arctic (region defined in Fig. 1a). It highlights the accelerated decline of the annual sea ice minimum and the major melting events that took place in 2007 and 2012 (Parkinson & Comiso, 2013). Most notably, the figure shows the rapid decline of MYI. During cold months, when blowing snow is most important, sea ice area has declined slightly but more importantly, FYI has increased, replacing older, less saline MYI. This results in increasing snow salinity in both the fixed salinity (MYI+FYI) and variable slinity (MYI+varFYI) blowing snow simulations (Fig. 4c). The increase in salinity is much stronger in theMYI+varFYI simulation because of the thinning snowpack on FYI (Fig. 4b). Salinity is highest in late fall when FYI begins to freeze, and the snowpack is thin. Salinity then decreases throughout the cold season as the snowpack becomes thicker. Decreasing snow depths in the Arctic (Fig 4b) are due to two processes: reduction in the MYI area so that a smaller MYI sea ice area is present during the high snowfall months of September and October (Boisvert et al., 2018; Mallett et al., 2021); and also freeze-up commences later, so a lower FYI area is available in these months, and more precipitation falls directly into the ocean (Mallett et al., 2021; Markus et al., 2009; Stroeve et al., 2020; Stroeve & Notz, 2018; Webster et al., 2014).

Figure 5 shows the spatial and temporal evolution of seasonally averaged snow depths for 1980-2017. We separate winter (Nov-Jan) and spring (Feb-Apr) months. At the beginning of the time period (1980-1984, Fig. 5ab) most of the Arctic sea ice is dominated by snow depths greater than 15-20 cm in winter (>25 cm in spring). At the end of the period (2013-2017) these deeper snow depths are limited to the central Arctic, with very thin snow depths (<15 cm) occurring in the East Siberian, Laptev, Chukchi, and Beaufort Seas, mostly constrained to FYI. We find that mean Arctic snow depths over sea ice have decreased at a rate of -0.79 cm/decade (-4%/decade)

during winter (Fig. 5e) and -0.98 cm/decade (-3.5%/decade) during spring (Fig. 5j). The largest negative trends (-4 to -6 cm decade^{-1}) occur in areas where FYI has replaced MYI (Fig 4 b-c, f-h), in the Beaufort, Chukchi, East Siberian, and Laptev Seas. In some regions, such as the Central Arctic, snow depth trends are positive but are not statistically significant. These trends in snow depths from SnowModel-LG are discussed in more detail in Stroeve et al. (2020) and are consistent with Webster et al. (2014).

Figure 6 shows the spatial and temporal evolution of snow salinity. Over the 1980-2017 period, we find that winter snow salinity in the variable salinity (MYI+varFYI) simulation increases by 36%/decade (0.027 psu/decade) while the salinity in the MYI+FYI simulation increases by 11%/decade (0.0047 psu/decade, Fig 5e). Similar trends occur in spring. These trends are significant. The largest increases in salinity occur in regions where FYI has replaced MYI and where snow depths are thinning, such as the East Siberian, Laptev, Kara, and Barents Seas (Fig 5di). By comparison between these two simulations, we infer that 1/3 of the increase in the OO+MYI+varFYI salinity is due to increasing FYI, with the remaining 2/3 due to thinning snow depths.

4 Changing Arctic SSA emissions and surface mass concentrations

SSA emissions from blowing snow have a near-linear dependence on the salinity of snow. Due to the rapid loss of MYI, increasing FYI, thinning snow depths and the resulting increase in snow salinity, we find that SSA emissions are increasing during the cold season. Figure 7(a-c, f-h) contrasts the OO+MYI+varFYI SSA emissions for 1980-1984 and 2013-2017, most notably highlighting areas with increasing FYI where emissions increased by a factor of 2-5 for winter-spring. Figure 7d shows the spatial variations of SSA emissions trends. The areas where the

trend is > 25% decade^{-1} are areas where FYI has replaced MYI and are consistent with the areas that show the largest decreases in snow depth and increases in snow salinity.

Averaged over the Arctic region, winter and spring open ocean (OO) SSA emissions are increasing at a rate of +8.7 and +6.5% decade^{-1} (0.11 and 0.15 Tg decade^{-1}), respectively (Fig 7e,j). This is due to a larger fraction of open water. The OO+MYI simulation displays a weaker trend (7-5% decade^{-1}), indicating that blowing snow SSA emissions from MYI are decreasing (Fig. 7 e,j). Adding blowing snow SSA emissions from FYI, the model predicts that total SSA emissions increase at a rate of 9.6-7.5 % decade^{-1} during winter-spring in the OO+MYI+varFYI simulation and 8.6-6.2% decade^{-1} in the OO+MYI+FYI simulation (Fig. 7e, j). During Winter, a large fraction of the increase in SSA emissions in the OO+MYI+varFYI (0.15 Tg decade^{-1}) is due to OO (0.11 Tg decade^{-1}), which thus account for 73% of SSA emissions increase. Similarly, during spring OO accounts for 62% of the increase. This is because OO emissions dominate supermicron emissions. Focusing on submicron SSA emissions, OO emissions only account for 40% of the SSA emission increase in winter and 16% of the emission increase in spring (Fig S1).

During the warm months, May-October, we also find that SSA emissions are increasing. During summer (fall) SSA emissions are increasing by 14% (12%) decade^{-1} due to increasing open ocean emissions as sea ice extent decreases.

This pan-Arctic increase in SSA emissions in the OO+MYI+varFYI simulation results in an increase in surface SSA mass concentrations at a rate of 12-8 % decade^{-1} (0.37-0.21 μg m^{-3}) in winter-spring (Fig. 8ej). The OO+MYI+FYI simulation predicts a smaller increase of 11-6 % decade^{-1} (0.28-0.12 μg m^{-3}). Figure 8 (a,f) shows that in 1980-1984 surface SSA mass

concentrations over sea ice range from 1.5-2.5 μg m^{-3} over large areas, while by 2013-2017 concentrations over most of the Arctic exceed 2.5 μg m^{-3}. The surface mass concentrations in the East Siberian and Chukchi seas increased by a factor of 2 or 15-25% $decade^{-1}$ (Fig. 8d). While the Central Arctic is dominated by MYI, trends > 5% $decade^{-1}$ are quite widespread throughout the region due to the transport of SSA emitted by blowing snow over FYI. We also find statically significant trends during summer and fall (Fig. 8ot): 7-11 % $decade^{-1}$ (0.064-0.19 μg m^{-3}).

During winter, SSA mass concentrations due to open ocean (OO) emissions show a positive trend of 12%/decade, due to increased ocean area from decreasing MYI and delayed freeze up of FYI (fig. 8e). This positive trend counteracts the negative trend of MYI SSA surface mass concentrations in the winter, leading to nearly constant SSA from OO+MYI. During the spring, when delayed freeze up of sea ice no longer impacts OO emissions, there is a much smaller trend (2.5%/decade). This results in a statistically significant negative trend in MYI+OO due to decreasing MYI emissions (Fig. 8e).

5 Observed long-term trends in SSA mass concentrations at Alert

Alert is the only Arctic site with SSA mass concentration observations over the entire 1980-2017 period, allowing us to compare observed and simulated trends. We find that observations at Alert display positive trends of +12% $decade^{-1}$ (+0.11 μg m^{-3} $decade^{-1}$) in winter and +9.6% $decade^{-1}$ (+0.07 μg m^{-3} $decade^{-1}$) in spring (Fig. 9ab). These trends are significant (Winter p=0.005, Spring p=0.03). When sampling GEOS-Chem at Alert, both the OO+MYI+FYI and OO+MYI+varFYI simulations do a reasonably good job at capturing the observed interannual variability (OO+MYI+varFYI Winter r=0.74, Spring r=0.59; OO+MYI+FYI Winter r=0.66, Spring r=0.65). These simulations predict increasing SSA mass concentrations, however the

magnitude of the trends is a factor of 2-3 smaller than observed and not statistically significant. When examining the broader region surrounding Alert (Fig. 8di), simulated trends are higher (10-15% decade^{-1}) and more consistent with observations. The weaker trends in the model at Alert relative to the modeled trends in the broader region surrounding Alert could be due to local topography effects in the model.

During Summer (May-Jul) observations show no trends, while the GEOS-Chem model displays weak increasing trends (<2%) that are not significant (Fig. 9c). During Fall (Aug-Sep), observations have a decreasing trend of -18% decade^{-1} (-0.036 μg m^{-3} decade^{-1}), which is significant. The model simulation also predicts a decreasing trend in Fall, however, it is weaker (–4.7% decade $^{-1}$ to –6.3% decade^{-1}) and not significant. Fig 8s shows that in Fall the model predicts that Alert is in a region of decreasing trends that extends from the Queen Elizabeth Islands to the north of Greenland. This is mainly due to decreasing MYI and the delayed freeze up of FYI in the fall.

In contrast with our results, Schmale et al. (2022) analyzed observations of Na^+ from Alert but found no statistically significant trends ($p>0.1$) for the 1980-2017 period. While we use the same statistical method (Mann–Kendall Theil–Sen method) to calculate trends, our studies differ in the periods examined: Schmale et a. (2022) divided the year into the haze season (January, February, March, April) and the summer season (June, July, August, September). Furthermore, they used seasonal median values, while we use seasonal mean values for winter (November, December, January), and spring (February, March, April).

6 Conclusions

We implemented spatially and temporally varying surface snow salinity in the GEOS-Chem global chemical transport model to better represent the effect of sea ice age and snow depth on SSA emissions from blowing snow. We used four datasets of snow salinity observations to develop a model that predicts surface snow salinity as a function of snow depth using the SnowModel-LG dataset. We conducted two blowing-snow simulations over a 38-year period, one with fixed salinity and the other using the spatiality and temporally varying snow salinity for FYI to evaluate the effects of decreasing sea ice age, extent, and snow depth on SSA emissions. Both simulations were successful in reproducing the observed seasonal cycle and cold season enhancement of SSA mass concentrations at Arctic sites. We note that the observations of SSA mass concentrations are limited to areas where the two blowing snow simulations are quite similar and lack observations in areas where the simulations differ. Therefore, we cannot conclude if one simulation performs better Arctic wide.

We find that cold season pan-Arctic SSA emissions are increasing at a rate of 9.6-7.5% decade^{-1} (winter-spring) in the varying salinity simulation. These trends in emissions are driven by a combination of decreasing sea ice extent (increasing open ocean emissions), replacement of less saline snow on MYI with more saline snow on FYI, and decreasing snow depths on FYI. When taking into account the snow-depth dependent salinity on FYI, our simulation predicts a +36-31 % decade^{-1} (0.03-0.02 psu decade^{-1}) increase in surface snow salinity, with the largest trends in the East Siberian, Laptev, Chukchi, and Beaufort Seas.

Both blowing snow simulations predicted statistically significant positive trends in SSA surface mass concentrations during the cold season. Our varying salinity simulation predicts that SSA surface mass concentrations have increased +12% decade^{-1} (+7.9% decade^{-1}) in winter (spring)

over the 1980-2017 period. The fixed salinity simulation predicts surface mass concentrations have increased +11% decade^{-1} (+5.6% decade^{-1}) in winter (spring). These increases are driven by increasing emissions from blowing snow. Observations at Alert display increasing trends of very similar magnitudes: +12% decade^{-1} in winter and +9.6% decade^{-1} in spring. When we sample the model directly at Alert, the model fails to capture the magnitude of the observed trend, but can reproduce the correct sign of the trend and the inter-annual variability quite well.

Our simulations predict that warm season SSA mass concentrations are also increasing over the Arctic, at a rate of +7.2% decade^{-1} in May-Jul and +11% decade^{-1} in Aug-Oct. These increases are driven by reductions in sea ice extent and increasing open ocean SSA emissions.

While the impact of changing anthropogenic aerosol in the Arctic has been examined in several studies (Garrett et al., 2009; Jones et al., 2007; Kay & Gettelman, 2009; Quinn et al., 2008), the impact of changing SSA aerosols has not received as much attention. During the cold season, SSA can act as ice nuclei (DeMott et al., 2016; Wise et al., 2012). Thus, SSA from local sea ice sources could influence the formation, precipitation, and radiative forcing of mixed-phase and ice clouds and thus could influence downward longwave radiative forcing. SSA also plays an important role in the release of active bromine in polar spring contributing to bromine explosions and ozone depletion events (Choi et al., 2018; Kalnajs et al., 2013; Yang et al., 2010). A recent satellite study by Bougoudis et al. (2020) found that tropospheric BrO columns over Arctic sea ice have been increasing at a rate of +15% decade^{-1} during polar spring. They inferred from comparisons and correlations with sea ice age that the reported changes in the extent and magnitude of tropospheric BrO columns are moderately related to the increase in FYI extent in the Arctic north of 70ºN both temporally and spatially, with a correlation coefficient of 0.32. Our

finding of an increasing trend in springtime SSA concentrations over the Arctic could provide a potential explanation for this increasing BrO column trends, both by releasing active bromine to the atmosphere, but also maintaining high levels of BrO by allowing the fast recycling of sea salt bromide to reactive bromine (Abbatt et al., 2012; Fan & Jacob, 1992; Lehrer et al., 2004). Furthermore, the increasing salinity of surface snow could enhance the activation of bromine from the snowpack (Simpson et al., 2005; Pratt et al., 2013). Further study will be needed to quantitatively evaluate the impact of increasing SSA concentrations and surface snow salinity on Arctic bromine activation.

Data Availability

The EASE-Grid Sea Ice Age data is available online (https://nsidc.org/data/nsidc-0611/versions/4). Daily, 1 September 1980 through 31 July 2018, snow depths used in this paper are available at the National Snow and Ice Data Center (NSIDC), Boulder, Colorado USA: Liston, G. E., J. Stroeve, and P. Itkin; Lagrangian Snow Distributions for Sea-Ice Applications; http://dx.doi.org/10.5067/27A0P5M6LZBI.

Figures

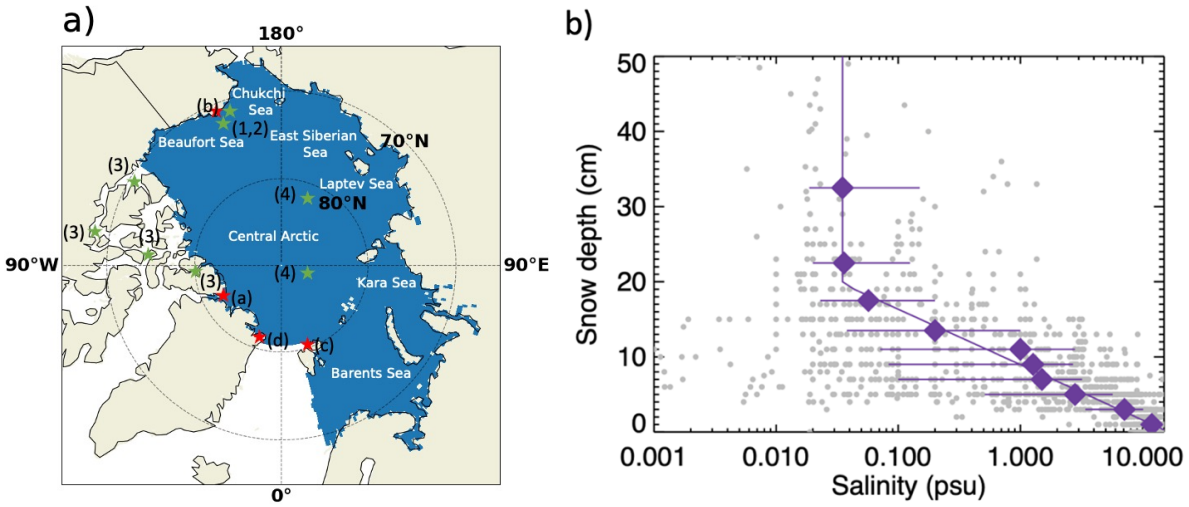

Figure 1: a) Locations of snow salinity observations (green stars: (1) Ewert et al., 2013; (2) Krnavek et al., 2012; (3) Nandan et al., 2017; (4) Peterson et al., 2019) and of the surface stations with sea salt mass concentrations observations (red stars: (a) Alert, (b) Barrow/Utqiaġvik, c) Zepplin, d) Villum) used in this study. The blue region constitutes the Arctic region considered in this study. This region includes the Kara, Barents, East Siberian, Laptev, Beaufort and Chukchi seas, and the Central Arctic. b) In situ observations of snow salinity (filled grey circles) as a function of snow depth. These observations were collected on FYI. 0 cm on the y-axis represents the snow/ice interface. The purple diamonds correspond to the medians of the observations separated into 2-5 cm snow thickness bins. Purple horizontal bars correspond to the 25th and 75th percentiles of each bin. The purple line is the fit to observations (Equation 1).

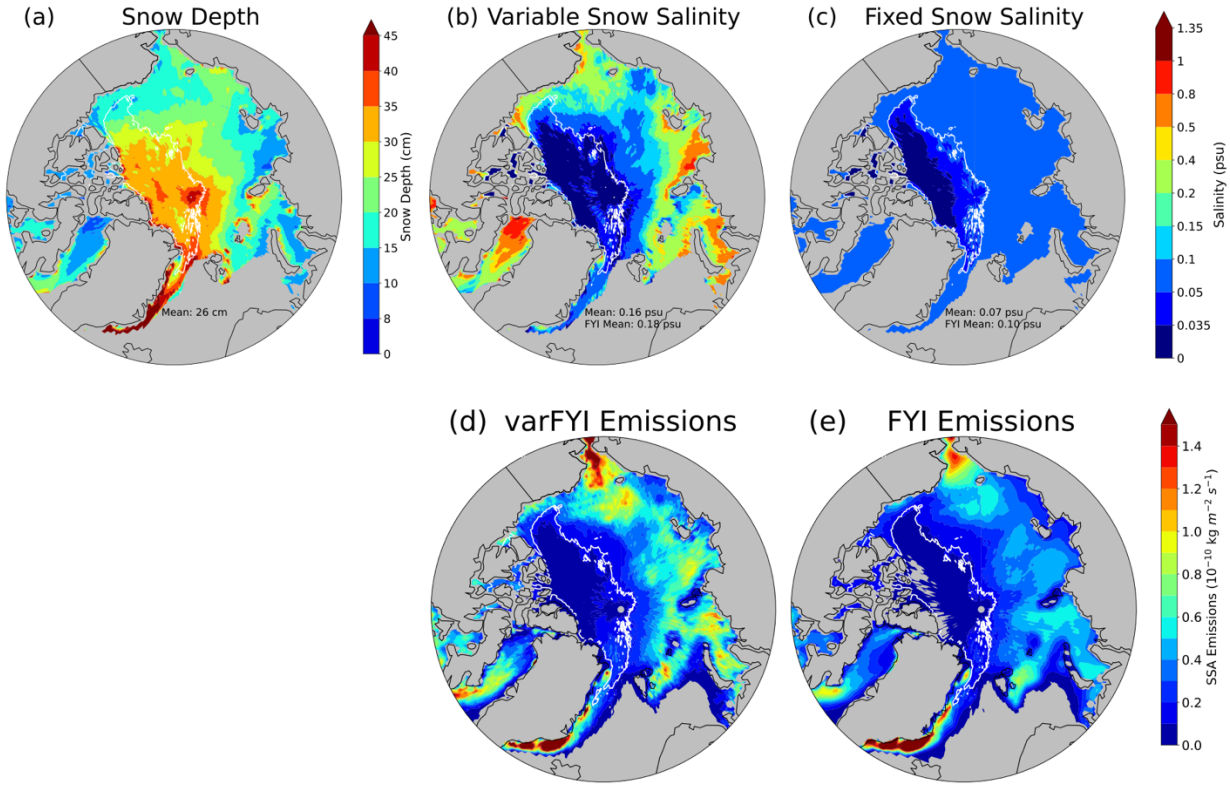

Figure 2. Spatial distribution of (a) SnowModel-LG snow depth over sea ice, (b) variable snow salinity calculated with Equation 1, (c) fixed snow salinity assuming 0.1 psu on FYI and 0.035 psu on MYI, (d) blowing snow SSA emissions from the variable salinity simulation (MYI+varFYI), and (e) blowing snow SSA emissions from the fixed salinity simulation (MYI+FYI) for February-April 2005-2014. The mean snow salinity excludes areas where snow depths are below the snow holding depth of 8 cm (see discussion in Section 2.3). The white contour represents mean MYI extent.

	OO			MYI			MYI+FYI			MYI+varFYI		
	0.01-0.5 µm	0.5-8 µm	Total	0.01-0.5 µm	0.5-8 µm	Total	0.01-0.5 µm	0.5-8 µm	Total	0.01-0.5 µm	0.5-8 µm	Total
Emission, Tg yr^{-1}	0.2	13.5	13.8	0.2	0.2	0.3	0.6	0.9	1.5	0.8	1.7	2.5
Dry Deposition, Tg yr^{-1}	0.0	4.3	4.3	0.04	0.1	0.1	0.1	0.3	0.4	0.1	0.6	0.8
Wet Deposition, Tg yr^{-1}	0.2	7.7	7.9	0.03	0.1	0.1	0.1	0.4	0.5	0.1	0.8	0.9
Lifetime, days	3.0	0.3	0.4	6.5	0.5	2.6	6.6	0.5	2.0	7.0	0.5	1.6
Burden, Gg	1.7	10.5	12.2	1.2	0.2	1.4	4.3	0.9	5.2	5.4	1.8	7.3
Surface Concentration, µg m^{-3}	0.2	1.4	1.5	0.2	0.0	0.3	0.6	0.2	0.8	0.8	0.4	1.2

Table 1. Annual mean Arctic (region defined in Fig. 1a) SSA budgets for SSA originating from the open ocean (OO), blowing snow over MYI (MYI), blowing snow over both MYI and FYI with fixed salinity (MYI+FYI), and blowing over MYI and FYI with variable salinity (MYI+varFYI) for 2005-2014.

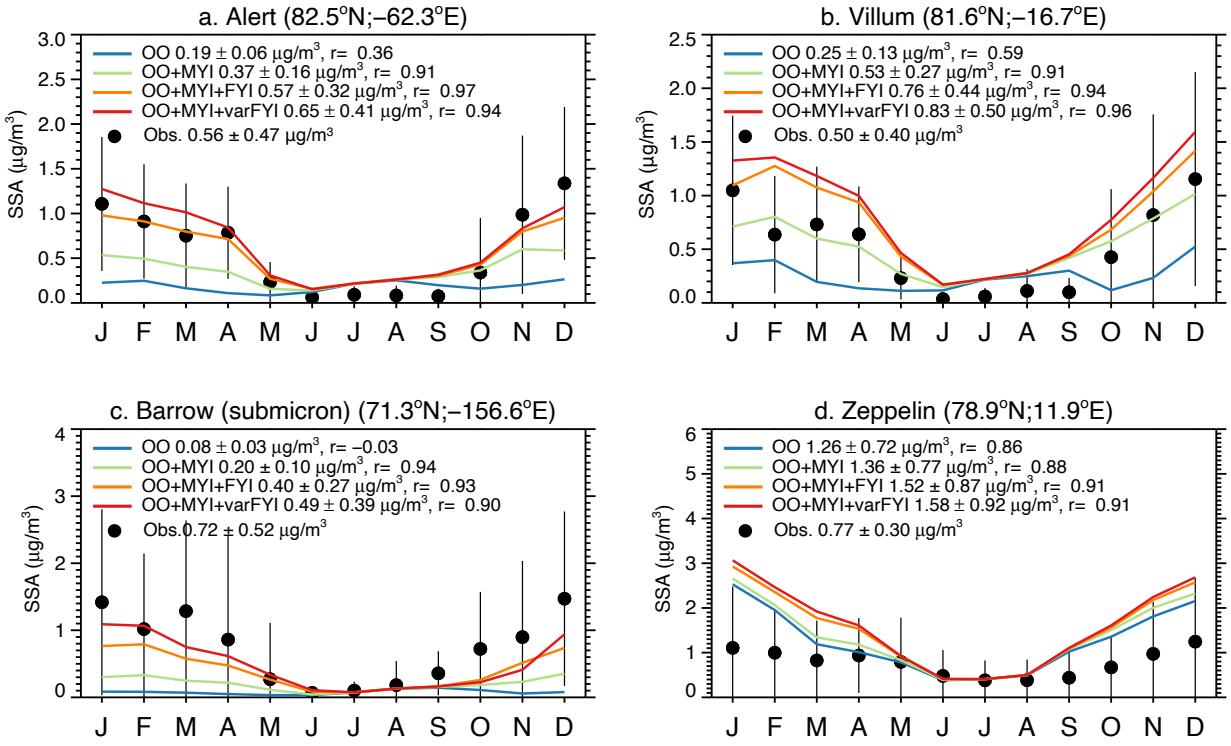

Figure 3. Monthly mean mass concentrations of SSA at: a) Alert, b) Villum, c) Barrow/Utqiaġvik, d) Zeppelin. All observations and model results are for 2005–2014 (except for Villum, where observations are available starting in 2008). The observed concentrations are indicated with filled black circles. The black vertical lines correspond to the standard deviations of monthly means for observations. The four GEOS-Chem simulations are shown with solid lines (OO: blue; OO+MYI: green, OO+MYI+FYI: orange; OO+MYI+varFYI: red). For each individual panel, the legend lists mean concentrations and standard deviations, as well as the correlation coefficient between model and observations.

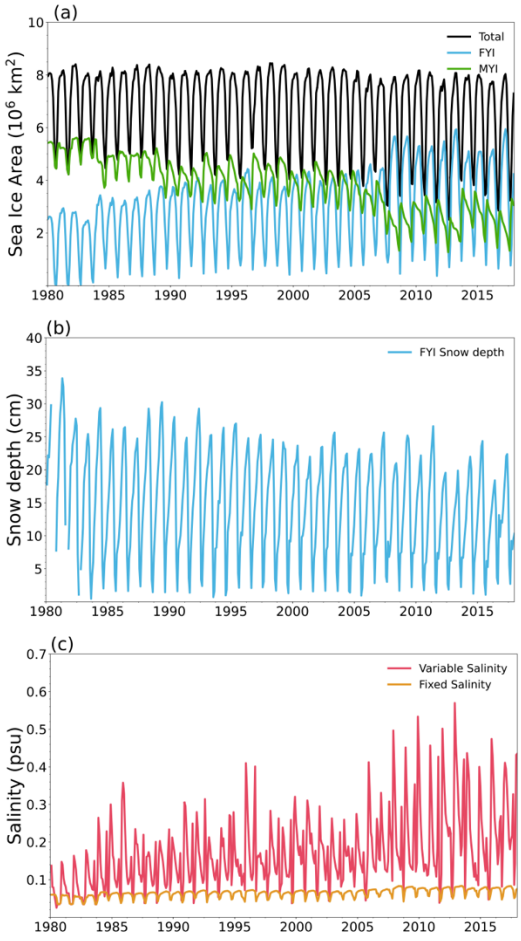

Figure 4. Monthly mean Arctic (a) sea ice area in units of 10^6 km^2, (b) snow depth over FYI in units of cm, and (c) surface snow salinity in units of psu (practical salinity units) for 1980-2017. The Arctic region is defined in Figure 1a. Panel (a) includes total sea ice area (black), FYI area (light blue), and MYI area (green). Panel (c) shows surface snow salinity for the fixed salinity (MYI+FYI) simulation (orange) and variable salinity (MYI+varFYI) simulation (red). Note that the MYI+varFYI salinity only includes regions with snow depth above the snow-holding depth of 8 cm (Section 2.3).

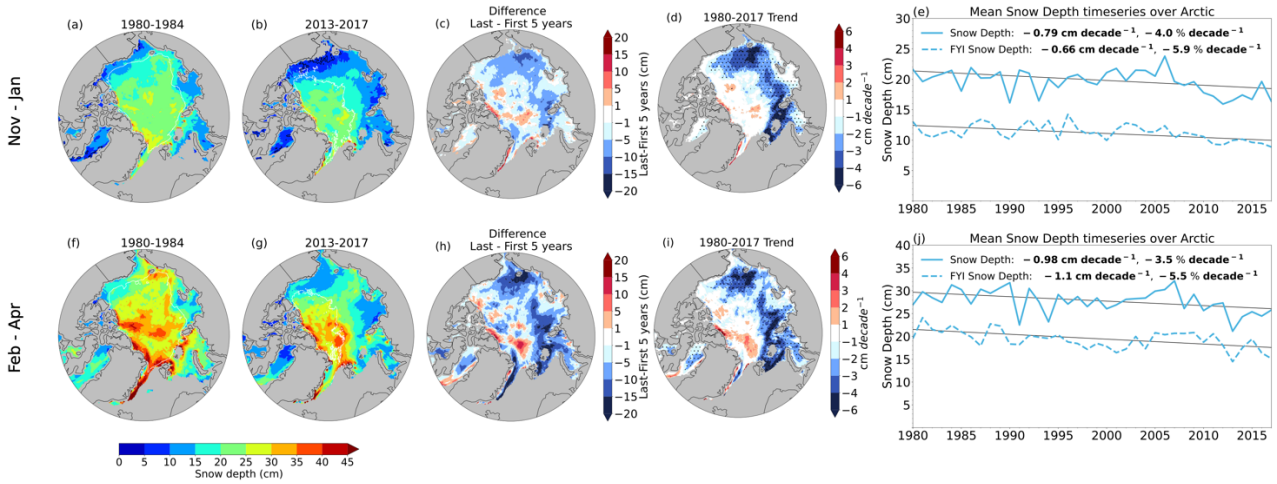

Figure 5 Seasonally averaged SnowModel-LG snow depths for winter (Nov-Jan; top row) and spring (Feb-Apr; bottom row). Average snow depth for (a, f) 1980-1984 and (b, g) 2013-2017, and (c, h) difference between the 2013-2017 and 1980-1984 snow depths. (d, i) Spatial distribution of trends (cm decade^{-1}) for 1980-2017. Black dots indicate statistically significant trends. The white contours on (a,b,f,g) show the mean extent of MYI. (e, j) Timeseries of Arctic snow depth over all sea ice (solid blue line) and FYI only (dashed blue line). The legend lists the trend in cm decade^{-1} and % decade^{-1}. Statistically significant trends are indicated in bold in the legend.

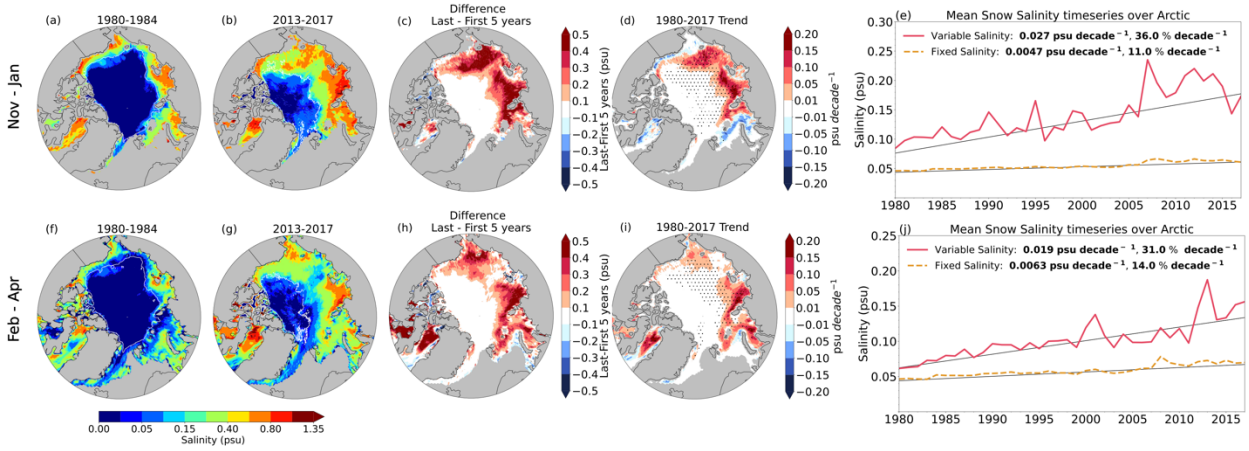

Figure 6. Seasonally averaged Arctic snow salinity on sea ice for winter (Nov-Jan; top row) and spring (Feb-Apr; bottom row) for the variable salinity simulation (MYI+varFYI). Average snow salinity for (a, f) 1980-1984 and (b, g) 2013-2017, and (c, h) difference between the 2013-2017 and 1980-1984 winter snow salinity. The white contours on (a,b,f,g) show the mean extent of MYI. (d, i) Spatial distribution of trends (psu decade^{-1}) for 1980-2017. Black dots indicate

statistically significant trends. (e,j) Timeseries of Arctic snow salinity using variable salinity (MYI+varFYI, red line) and fixed salinity (MYI+FYI, orange line). The legend lists the trend in psu decade^{-1} and % decade^{-1}. Statistically significant trends are indicated in bold in the legend.

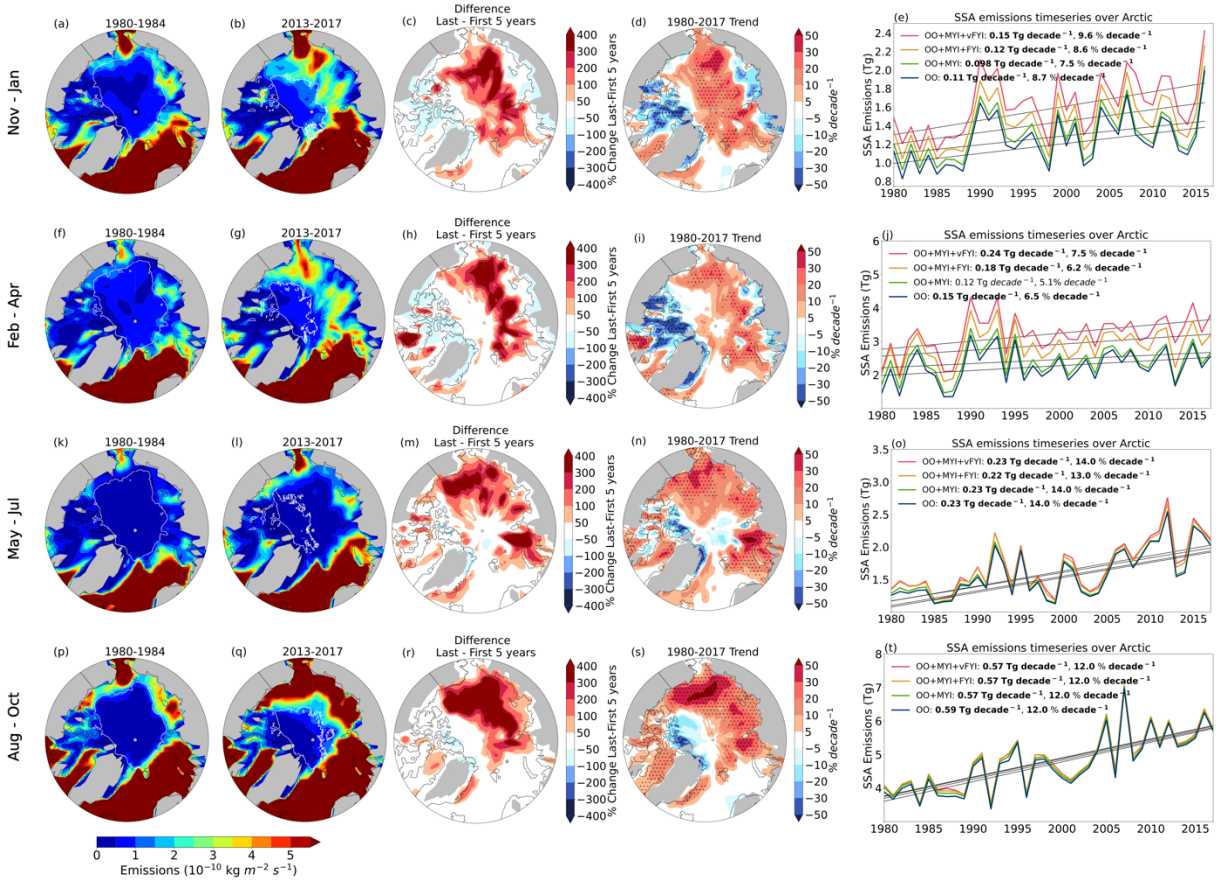

Figure 7. Seasonally averaged SSA emissions for winter (Nov-Jan; first row), spring (Feb-Apr; second row), summer (May-Jul; third row), and fall (Aug-Oct; fourth row) for the OO+MYI+varFYI simulation. The first three columns from the left indicate SSA emissions for 1980-1984, 2013-2017, and the difference between the 2013-2017 and 1980-1984 emissions. Panels d, i, n, s: Spatial distribution of 1980-2017 trends (% decade^{-1}). Rightmost column (panels e, j, o, t): 1980-2017 timeseries of seasonally averaged SSA emissions over the Arctic for four simulations: OO (blue line), OO+MYI (green line), OO+MYI+FYI (orange line), OO+MYI+varFYI (red line).

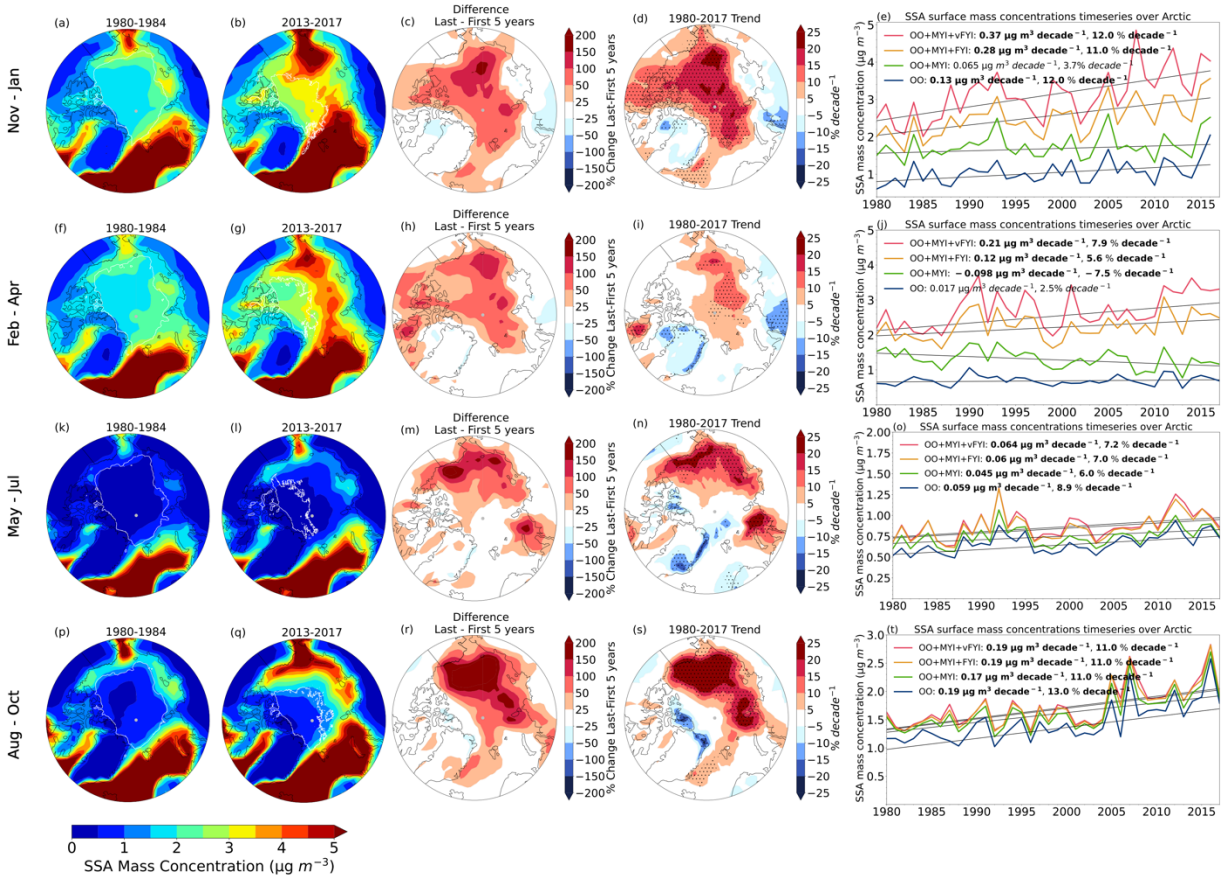

Figure 8: Same as Fig. 7 but for SSA mass concentrations at the surface.

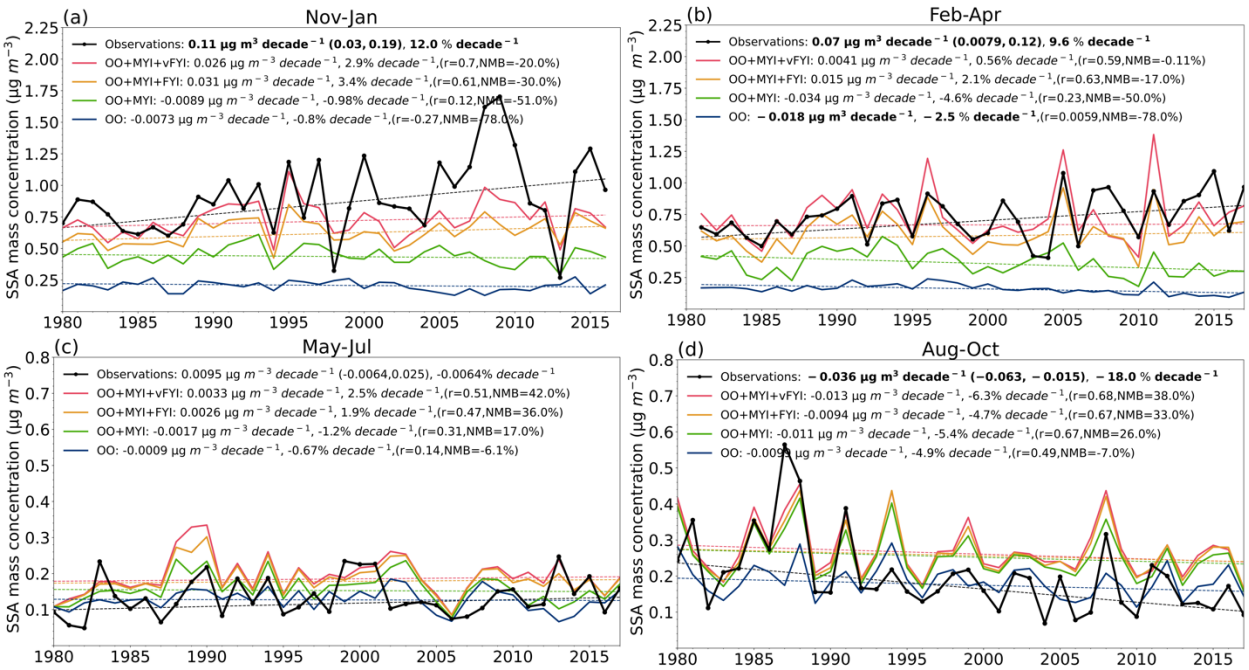

Figure 9. Seasonally averaged SSA surface mass concentrations at Alert, Canada in (a) Nov-Jan, (b) Feb-Apr, (c) May-Jul, and (d) Aug-Sep. Observations are shown in black, with black error bars indicating the standard deviation. Model results are shown for the: OO (blue line), OO+MYI (green line), OO+MYI+FYI (orange line), OO+MYI+varFYI (red line). For each panel, the legend lists the trend in μg m^{-3} (low, high) slope, and percent per decade, as well as the statistical significance (numbers in bold). For the model simulations, we include the correlation coefficient (r) and normalized mean bias (NMB) compared to observations.

Supplemental Figures

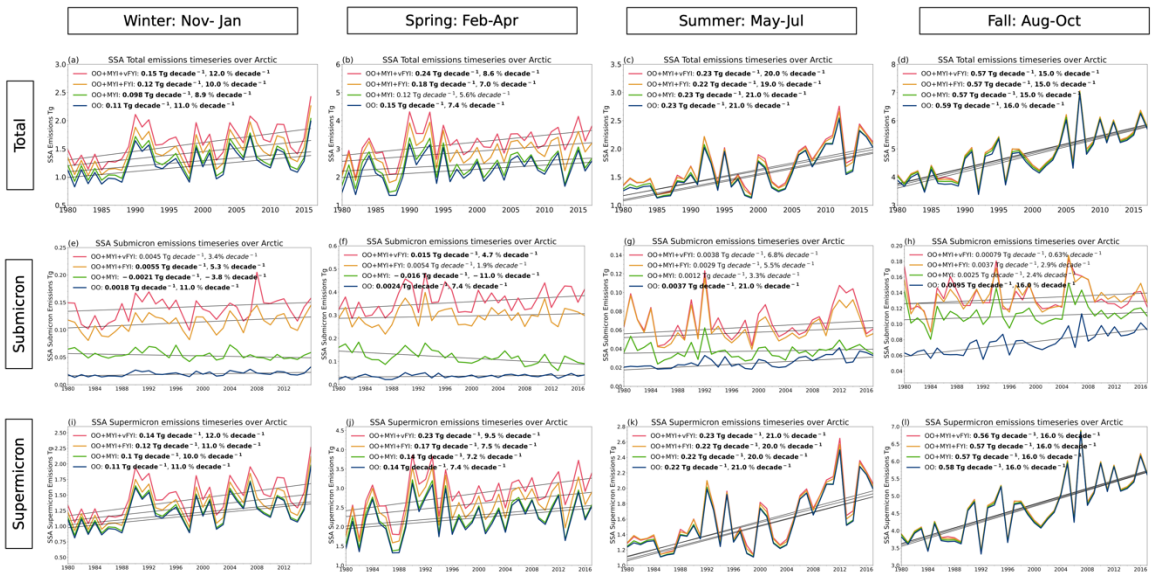

References

Abbatt, J. P. D., Richard Leaitch, W., Aliabadi, A. A., Bertram, A. K., Blanchet, J. P., Boivin-Rioux, A., Bozem, H., Burkart, J., Chang, R. Y. W., Charette, J., Chaubey, J. P., Christensen, R. J., Cirisan, A., Collins, D. B., Croft, B., Dionne, J., Evans, G. J., Fletcher, C. G., Gali, M., … Yakobi-Hancock, J. D. (2019). Overview paper: New insights into aerosol and climate in the Arctic. *Atmospheric Chemistry and Physics*, *19*(4). https://doi.org/10.5194/acp-19-2527-2019

Abbatt, J. P. D., Thomas, J. L., Abrahamsson, K., Boxe, C., Granfors, A., Jones, A. E., King, M. D., Saiz-Lopez, A., Shepson, P. B., Sodeau, J., Toohey, D. W., Toubin, C., von Glasow, R., Wren, S. N., & Yang, X. (2012). Halogen activation via interactions with environmental ice and snow in the polar lower troposphere and other regions. *Atmospheric Chemistry and Physics*, *12*(14), 6237–6271. https://doi.org/10.5194/acp-12-6237-2012

Alvarez-Aviles, L., Simpson, W. R., Douglas, T. A., Sturm, M., Perovich, D., & Domine, F. (2008). Frost flower chemical composition during growth and its implications for aerosol production and bromine activation. *Journal of Geophysical Research Atmospheres*, *113*(21). https://doi.org/10.1029/2008JD010277

Bey, I., Jacob, D. J., Yantosca, R. M., Logan, J. A., Field, B. D., Fiore, A. M., Li, Q., Liu, H. Y., Mickley, L. J., & Schultz, M. G. (2001). Global modeling of tropospheric chemistry with assimilated meteorology: Model description and evaluation. *Journal of Geophysical Research Atmospheres*, *106*(D19). https://doi.org/10.1029/2001JD000807

Boisvert, L. N., Webster, M. A., Petty, A. A., Markus, T., Bromwich, D. H., & Cullather, R. I. (2018). Intercomparison of precipitation estimates over the Arctic ocean and its peripheral seas from reanalyses. *Journal of Climate*, *31*(20). https://doi.org/10.1175/JCLI-D-18-0125.1

Bougoudis, I., Blechschmidt, A. M., Richter, A., Seo, S., Burrows, J. P., Theys, N., & Rinke, A. (2020). Long-term time series of Arctic tropospheric BrO derived from UV-VIS satellite remote sensing and its relation to first-year sea ice. *Atmospheric Chemistry and Physics*. https://doi.org/10.5194/acp-20-11869-2020

Browse, J., Carslaw, K. S., Mann, G. W., Birch, C. E., Arnold, S. R., & Leck, C. (2014). The complex response of Arctic aerosol to sea-ice retreat. *Atmospheric Chemistry and Physics*, *14*(14). https://doi.org/10.5194/acp-14-7543-2014

Budd, W. F. (2013). *The Drifting of Nonuniform Snow Particles 1* . https://doi.org/10.1029/ar009p0059

Choi, S., Theys, N., Salawitch, R. J., Wales, P. A., Joiner, J., Canty, T. P., Chance, K., Suleiman, R. M., Palm, S. P., Cullather, R. I., Darmenov, A. S., da Silva, A., Kurosu, T. P., Hendrick, F., & van Roozendael, M. (2018). Link Between Arctic Tropospheric BrO Explosion Observed From Space and Sea-Salt Aerosols From Blowing Snow Investigated Using Ozone Monitoring Instrument BrO Data and GEOS-5 Data Assimilation System. *Journal of Geophysical Research: Atmospheres*. https://doi.org/10.1029/2017JD026889

Collaud Coen, M., Andrews, E., Bigi, A., Martucci, G., Romanens, G., Vogt, F. P. A., & Vuilleumier, L. (2020). Effects of the prewhitening method, the time granularity, and the time segmentation on the Mann-Kendall trend detection and the associated Sen's slope. *Atmospheric Measurement Techniques*, *13*(12). https://doi.org/10.5194/amt-13-6945-2020

Collaud Coen, M., Andrews, E., Lastuey, A., Petkov Arsov, T., Backman, J., Brem, B. T., Bukowiecki, N., Couret, C., Eleftheriadis, K., Flentje, H., Fiebig, M., Gysel-Beer, M., Hand, J. L., Hoffer, A., Hooda, R., Hueglin, C., Joubert, W., Keywood, M., Eun Kim, J., … Laj, P. (2020). Multidecadal trend analysis of in situ aerosol radiative properties around the world. *Atmospheric Chemistry and Physics*, *20*(14). https://doi.org/10.5194/acp-20-8867-2020

Cox, G. F. N., & Weeks, W. F. (1974). Salinity Variations in Sea Ice. *Journal of Glaciology*, *13*(67), 109–120. https://doi.org/10.3189/S0022143000023418

de Leeuw, G., Andreas, E. L., Anguelova, M. D., Fairall, C. W., Lewis, E. R., O'Dowd, C., Schulz, M., & Schwartz, S. E. (2011). Production flux of sea spray aerosol. *Reviews of Geophysics*, *49*(2). https://doi.org/10.1029/2010RG000349

DeMott, P. J., Hill, T. C. J., McCluskey, C. S., Prather, K. A., Collins, D. B., Sullivan, R. C., Ruppel, M. J., Mason, R. H., Irish, V. E., Lee, T., Hwang, C. Y., Rhee, T. S., Snider, J. R., McMeeking, G. R., Dhaniyala, S., Lewis, E. R., Wentzell, J. J. B., Abbatt, J., Lee, C., … Franc, G. D. (2016). Sea spray aerosol as a unique source of ice nucleating particles. *Proceedings of the National Academy of Sciences of the United States of America*, *113*(21). https://doi.org/10.1073/pnas.1514034112

Déry, S. J., & Yau, M. K. (1999). A bulk blowing snow model. *Boundary-Layer Meteorology*, *93*(2). https://doi.org/10.1023/A:1002065615856

Domine, F., Sparapani, R., Ianniello, A., & Beine, H. J. (2004). The origin of sea salt in snow on Arctic sea ice and in coastal regions. *Atmospheric Chemistry and Physics*, *4*(9–10). https://doi.org/10.5194/acp-4-2259-2004

Donlon, C. J., Martin, M., Stark, J., Roberts-Jones, J., Fiedler, E., & Wimmer, W. (2012). The Operational Sea Surface Temperature and Sea Ice Analysis (OSTIA) system. *Remote Sensing of Environment*, *116*. https://doi.org/10.1016/j.rse.2010.10.017

Drinkwater, M. R., & Crocker, G. B. (1988). Modelling changes in the dielectric and scattering properties of young snow-covered sea ice at GHz frequencies. *Journal of Glaciology*, *34*(118). https://doi.org/10.3189/s0022143000007012

Ewert, M., Carpenter, S. D., Colangelo-Lillis, J., & Deming, J. W. (2013). Bacterial and extracellular polysaccharide content of brine-wetted snow over Arctic winter first-year sea ice. *Journal of Geophysical Research: Oceans*. https://doi.org/10.1002/jgrc.20055

Fan, S. M., & Jacob, D. J. (1992). Surface ozone depletion in Arctic spring sustained by bromine reactions on aerosols. *Nature*, *359*(6395). https://doi.org/10.1038/359522a0

Fisher, J. A., Jacob, D. J., Wang, Q., Bahreini, R., Carouge, C. C., Cubison, M. J., Dibb, J. E., Diehl, T., Jimenez, J. L., Leibensperger, E. M., Lu, Z., Meinders, M. B. J., Pye, H. O. T., Quinn, P. K., Sharma, S., Streets, D. G., van Donkelaar, A., & Yantosca, R. M. (2011). Sources, distribution, and acidity of sulfate-ammonium aerosol in the Arctic in winter-spring. *Atmospheric Environment*, *45*(39). https://doi.org/10.1016/j.atmosenv.2011.08.030

Fox-Kemper, B., Hewitt, H., Xiao, C., Aðalgeirsdóttir, G., Drijfhout, S., Edwards, T., Golledge, N., Hemer, M., Kopp, R., Krinner, G., Mix, A., Notz, D., Nowiciki, S., Nurhati, I., Ruiz, J., Sallée, J., Slangen, A., & Yu, Y. (2021). Ocean, Cryosphere and Sea Level Change. *Climate Change 2021: The Physical Science Basis. Contribution of Working Group I to the Sixth Assessment Report of the Intergovernmental Panel on Climate ChangeScience Basis. Contribution of Working Group I to the Sixth Assessment Report of the Intergover*, *2018*(August).

Freud, E., Krejci, R., Tunved, P., Leaitch, R., Nguyen, Q. T., Massling, A., Skov, H., & Barrie, L. (2017). Pan-Arctic aerosol number size distributions: Seasonality and transport patterns. *Atmospheric Chemistry and Physics*, *17*(13). https://doi.org/10.5194/acp-17-8101-2017

Frey, M., Norris, S., Brooks, I., Anderson, P., Nishimura, K., Yang, X., Jones, A., Nerentorp Mastromonaco, M., Jones, D., & Wolff, E. (2019). First direct observation of sea salt aerosol production from blowing snow above sea ice. *Atmospheric Chemistry and Physics*. https://doi.org/10.5194/acp-2019-259

Garrett, T. J., Maestas, M. M., Krueger, S. K., & Schmidt, C. T. (2009). Acceleration by aerosol of a radiative-thermodynamic cloud feedback influencing Arctic surface warming. *Geophysical Research Letters*, *36*(19). https://doi.org/10.1029/2009GL040195

Gelaro, R., McCarty, W., Suárez, M. J., Todling, R., Molod, A., Takacs, L., Randles, C. A., Darmenov, A., Bosilovich, M. G., Reichle, R., Wargan, K., Coy, L., Cullather, R., Draper, C., Akella, S., Buchard, V., Conaty, A., da Silva, A. M., Gu, W., … Zhao, B. (2017). The modern-era retrospective analysis for research and applications, version 2 (MERRA-2). *Journal of Climate*. https://doi.org/10.1175/JCLI-D-16-0758.1

Gilgen, A., Ting Katty Huang, W., Ickes, L., Neubauer, D., & Lohmann, U. (2018). How important are future marine and shipping aerosol emissions in a warming Arctic summer and autumn? *Atmospheric Chemistry and Physics*, *18*(14). https://doi.org/10.5194/acp-18-10521-2018

Heslin-Rees, D., Burgos, M., Hansson, H. C., Krejci, R., Ström, J., Tunved, P., & Zieger, P. (2020). From a polar to a marine environment: Has the changing Arctic led to a shift in aerosol light scattering properties? *Atmospheric Chemistry and Physics*, *20*(21). https://doi.org/10.5194/acp-20-13671-2020

Huang, J., & Jaeglé, L. (2017). Wintertime enhancements of sea salt aerosol in polar regions consistent with a sea ice source from blowing snow. *Atmospheric Chemistry and Physics*, *17*(5). https://doi.org/10.5194/acp-17-3699-2017

Huang, J., Jaeglé, L., Chen, Q., Alexander, B., Sherwen, T., Evans, M. J., Theys, N., & Choi, S. (2020). Evaluating the impact of blowing-snow sea salt aerosol on springtime BrO and O3 in the Arctic. *Atmospheric Chemistry and Physics*, *20*(12), 7335–7358. https://doi.org/10.5194/acp-20-7335-2020

Huang, J., Jaeglé, L., & Shah, V. (2018). Using CALIOP to constrain blowing snow emissions of sea salt aerosols over Arctic and Antarctic sea ice. *Atmospheric Chemistry and Physics*, *18*(22), 16253–16269. https://doi.org/10.5194/acp-18-16253-2018

Jaeglé, L., Quinn, P. K., Bates, T. S., Alexander, B., & Lin, J. T. (2011). Global distribution of sea salt aerosols: New constraints from in situ and remote sensing observations. *Atmospheric Chemistry and Physics*, *11*(7). https://doi.org/10.5194/acp-11-3137-2011

Jones, A., Haywood, J. M., & Boucher, O. (2007). Aerosol forcing, climate response and climate sensitivity in the Hadley Centre climate model. *Journal of Geophysical Research Atmospheres*, *112*(20). https://doi.org/10.1029/2007JD008688

Kaleschke, L., Richter, A., Burrows, J., Afe, O., Heygster, G., Notholt, J., Rankin, A. M., Roscoe, H. K., Hollwedel, J., Wagner, T., & Jacobi, H. W. (2004). Frost flowers on sea ice as a source of sea salt and their influence on tropospheric halogen chemistry. *Geophysical Research Letters*. https://doi.org/10.1029/2004GL020655

Kalnajs, L. E., Avallone, L. M., & Toohey, D. W. (2013). Correlated measurements of ozone and particulates in the Ross Island region, Antarctica. *Geophysical Research Letters*, *40*(23). https://doi.org/10.1002/2013GL058422

Kay, J. E., & Gettelman, A. (2009). Cloud influence on and response to seasonal Arctic sea ice loss. *Journal of Geophysical Research Atmospheres*, *114*(18). https://doi.org/10.1029/2009JD011773

Keller, C. A., Long, M. S., Yantosca, R. M., da Silva, A. M., Pawson, S., & Jacob, D. J. (2014). HEMCO v1.0: A versatile, ESMF-compliant component for calculating emissions in atmospheric models. *Geoscientific Model Development*. https://doi.org/10.5194/gmd-7-1409-2014

Krnavek, L., Simpson, W. R., Carlson, D., Domine, F., Douglas, T. A., & Sturm, M. (2012). The chemical composition of surface snow in the Arctic: Examining marine, terrestrial, and atmospheric influences. *Atmospheric Environment*. https://doi.org/10.1016/j.atmosenv.2011.11.033

Kwok, R. (2018). Arctic sea ice thickness, volume, and multiyear ice coverage: Losses and coupled variability (1958-2018). In *Environmental Research Letters* (Vol. 13, Issue 10). https://doi.org/10.1088/1748-9326/aae3ec

Langlois, A., & Barber, D. G. (2007). Passive microwave remote sensing of seasonal snow-covered sea ice. In *Progress in Physical Geography* (Vol. 31, Issue 6). https://doi.org/10.1177/0309133307087082

Lehrer, E., Hönninger, G., & Platt, U. (2004). A one dimensional model study of the mechanism of halogen liberation and vertical transport in the polar troposphere. *Atmospheric Chemistry and Physics*, *4*(11–12). https://doi.org/10.5194/acp-4-2427-2004

Lewis, E. R., & Schwartz, S. E. (2004). Sea salt aerosol production: Mechanisms, methods, measurements and models—A critical review. In *Geophysical Monograph Series* (Vol. 152). https://doi.org/10.1029/152GM01

Liston, G. E., Itkin, P., Stroeve, J., Tschudi, M., Stewart, J. S., Pedersen, S. H., Reinking, A. K., & Elder, K. (2020). A Lagrangian Snow-Evolution System for Sea-Ice Applications (SnowModel-LG): Part I—Model Description. *Journal of Geophysical Research: Oceans*, *125*(10). https://doi.org/10.1029/2019JC015913

Liston, G. E., & Sturm, M. (2002). Winter precipitation patterns in arctic Alaska determined from a blowing-snow model and snow-depth observations. *Journal of Hydrometeorology*, *3*(6). https://doi.org/10.1175/1525-7541(2002)003<0646:WPPIAA>2.0.CO;2

Liu, H., Jacob, D. J., Bey, I., & Yantosca, R. M. (2001). Constraints from 210Pb and 7Be on wet deposition and transport in a global three-dimensional chemical tracer model driven by assimilated meteorological fields. *Journal of Geophysical Research Atmospheres*, *106*(D11). https://doi.org/10.1029/2000JD900839

Mallett, R. D. C., Stroeve, J. C., Tsamados, M., Landy, J. C., Willatt, R., Nandan, V., & Liston, G. E. (2021). Faster decline and higher variability in the sea ice thickness of the marginal Arctic seas when accounting for dynamic snow cover. *Cryosphere*, *15*(5). https://doi.org/10.5194/tc-15-2429-2021

Mann, G. W., Anderson, P. S., & Mobbs, S. D. (2000). Profile measurements of blowing snow at Halley, Antarctica. *Journal of Geophysical Research Atmospheres*, *105*(D19). https://doi.org/10.1029/2000JD900247

Marelle, L., Thomas, J. L., Ahmed, S., Tuite, K., Stutz, J., Dommergue, A., Simpson, W. R., Frey, M. M., & Baladima, F. (2021). Implementation and Impacts of Surface and Blowing Snow Sources of Arctic Bromine Activation Within WRF-Chem 4.1.1. *Journal of Advances in Modeling Earth Systems*, *13*(8). https://doi.org/10.1029/2020MS002391

Markus, T., Stroeve, J. C., & Miller, J. (2009). Recent changes in Arctic sea ice melt onset, freezeup, and melt season length. *Journal of Geophysical Research: Oceans*, *114*(12). https://doi.org/10.1029/2009JC005436

Massom, R. A., Eicken, H., Haas, C., Jeffries, M. O., Drinkwater, M. R., Sturm, M., Worby, A. P., Wu, X., Lytle, V. I., Ushio, S., Morris, K., Reid, P. A., Warren, S. G., & Allison, I. (2001). Snow on Antarctic sea ice. *Reviews of Geophysics*, *39*(3). https://doi.org/10.1029/2000RG000085

Nandan, V., Geldsetzer, T., Yackel, J., Mahmud, M., Scharien, R., Howell, S., King, J., Ricker, R., & Else, B. (2017). Effect of Snow Salinity on CryoSat-2 Arctic First-Year Sea Ice Freeboard Measurements. *Geophysical Research Letters*. https://doi.org/10.1002/2017GL074506

Nilsson, E. D., Rannik, Ü., Swietlicki, E., Leck, C., Aalto, P. P., Zhou, J., & Norman, M. (2001). Turbulent aerosol fluxes over the Arctic Ocean 2. Wind-driven sources from the sea. *Journal of Geophysical Research Atmospheres*, *106*(D23). https://doi.org/10.1029/2000JD900747

Nishimura, K., & Nemoto, M. (2005). Blowing snow at Mizuho station, Antarctica. *Philosophical Transactions of the Royal Society A: Mathematical, Physical and Engineering Sciences*, *363*(1832). https://doi.org/10.1098/rsta.2005.1599

O'Dowd, C. D., Smith, M. H., Consterdine, I. E., & Lowe, J. A. (1997). Marine aerosol, sea-salt, and the marine sulphur cycle: A short review. *Atmospheric Environment*, *31*(1). https://doi.org/10.1016/S1352-2310(96)00106-9

Parkinson, C. L., & Comiso, J. C. (2013). On the 2012 record low Arctic sea ice cover: Combined impact of preconditioning and an August storm. *Geophysical Research Letters*, *40*(7). https://doi.org/10.1002/grl.50349

Perovich, D. K., & Richter-Menge, J. A. (1994). Surface characteristics of lead ice. *Journal of Geophysical Research*, *99*(C8). https://doi.org/10.1029/94jc01194

Peterson, P. K., Hartwig, M., May, N. W., Schwartz, E., Rigor, I., Ermold, W., Steele, M., Morison, J. H., Nghiem, S. v., & Pratt, K. A. (2019). Snowpack measurements suggest role for multi-year sea ice regions in Arctic atmospheric bromine and chlorine chemistry. *Elementa*, *7*(1). https://doi.org/10.1525/elementa.352

Quinn, P. K., Bates, T. S., Baum, E., Doubleday, N., Fiore, A. M., Flanner, M., Fridlind, A., Garrett, T. J., Koch, D., Menon, S., Shindell, D., Stohl, A., & Warren, S. G. (2008). Short-lived pollutants in the Arctic: Their climate impact and possible mitigation strategies. *Atmospheric Chemistry and Physics*, *8*(6). https://doi.org/10.5194/acp-8-1723-2008

Rankin, A. M., Wolff, E. W., & Martin, S. (2002). Frost flowers: Implications for tropospheric chemistry and ice core interpretation. *Journal of Geophysical Research Atmospheres*. https://doi.org/10.1029/2002JD002492

Reynolds, R. W., Smith, T. M., Liu, C., Chelton, D. B., Casey, K. S., & Schlax, M. G. (2007). Daily high-resolution-blended analyses for sea surface temperature. *Journal of Climate*, *20*(22). https://doi.org/10.1175/2007JCLI1824.1

Rhodes, R. H., Yang, X., Wolff, E. W., McConnell, J. R., & Frey, M. M. (2017). Sea ice as a source of sea salt aerosol to Greenland ice cores: A model-based study. *Atmospheric Chemistry and Physics*, *17*(15). https://doi.org/10.5194/acp-17-9417-2017

Roscoe, H. K., Brooks, B., Jackson, A. v., Smith, M. H., Walker, S. J., Obbard, R. W., & Wolff, E. W. (2011). Frost flowers in the laboratory: Growth, characteristics, aerosol, and the

underlying sea ice. *Journal of Geophysical Research Atmospheres*, *116*(12). https://doi.org/10.1029/2010JD015144

Schmale, J., Zieger, P., & Ekman, A. M. L. (2021). Aerosols in current and future Arctic climate. *Nature Climate Change*, *11*(2). https://doi.org/10.1038/s41558-020-00969-5

Sharma, S., Barrie, L. A., Magnusson, E., Brattström, G., Leaitch, W. R., Steffen, A., & Landsberger, S. (2019). A Factor and Trends Analysis of Multidecadal Lower Tropospheric Observations of Arctic Aerosol Composition, Black Carbon, Ozone, and Mercury at Alert, Canada. *Journal of Geophysical Research: Atmospheres*, *124*(24). https://doi.org/10.1029/2019JD030844

Simpson, W. R., von Glasow, R., Riedel, K., Anderson, P., Ariya, P., Bottenheim, J., Burrows, J., Carpenter, L. J., Frieß, U., Goodsite, M. E., Heard, D., Hutterli, M., Jacobi, H. W., Kaleschke, L., Neff, B., Plane, J., Platt, U., Richter, A., Roscoe, H., … Wolff, E. (2007). Halogens and their role in polar boundary-layer ozone depletion. *Atmospheric Chemistry and Physics*, *7*(16), 4375–4418. https://doi.org/10.5194/acp-7-4375-2007

Skov, H., Hjorth, J., Nordstrøm, C., Jensen, B., Christoffersen, C., Poulsen, M. B., Liisberg, J. B., Beddows, D., Dall'Osto, M., & Christensen, J. H. (2020). Variability in gaseous elemental mercury at villum research station, Station Nord, in North Greenland from 1999 to 2017. *Atmospheric Chemistry and Physics*, *20*(21). https://doi.org/10.5194/acp-20-13253-2020

Slinn, S. A., & Slinn, W. G. N. (1980). Predictions for particle deposition on natural waters. *Atmospheric Environment (1967)*, *14*(9). https://doi.org/10.1016/0004-6981(80)90032-3

Stroeve, J., Liston, G. E., Buzzard, S., Zhou, L., Mallett, R., Barrett, A., Tschudi, M., Tsamados, M., Itkin, P., & Stewart, J. S. (2020). A Lagrangian Snow Evolution System for Sea Ice Applications (SnowModel-LG): Part II—Analyses. *Journal of Geophysical Research: Oceans*, *125*(10). https://doi.org/10.1029/2019JC015900

Stroeve, J., & Notz, D. (2018). Changing state of Arctic sea ice across all seasons. In *Environmental Research Letters* (Vol. 13, Issue 10). https://doi.org/10.1088/1748-9326/aade56

Struthers, H., Ekman, A. M. L., Glantz, P., Iversen, T., Kirkevåg, A., Mårtensson, E. M., Seland, & Nilsson, E. D. (2011). The effect of sea ice loss on sea salt aerosol concentrations and the radiative balance in the Arctic. *Atmospheric Chemistry and Physics*, *11*(7). https://doi.org/10.5194/acp-11-3459-2011

Swanson, W. F., Holmes, C. D., Simpson, W. R., Confer, K. L., Marelle, L., Thomas, J. L., Jaeglé, L., Alexander, B., Zhai, S., Chen, Q., Wang, X., & Sherwen, T. (n.d.). *Comparison of model and ground observations finds snowpack and blowing snow both contribute to Arctic tropospheric reactive bromine*. Retrieved May 3, 2022, from https://acp.copernicus.org/preprints/acp-2022-44/

Taylor, K. E., Williamson, D. L., & Zwiers, F. W. (2000). The Sea Surface Temperature and Sea-Ice Concentration Boundary Conditions for AMIP II Simulations. *PCMDI Report Series*, *60*.

TOPPING, G. (1972). Introduction to marine chemistry By J. P. Riley and R. Chester. Pp xiv + 465. Academic Press Inc., London and New York. 1971. E6a00. *Endeavour*, *31*(112). https://doi.org/10.1016/0160-9327(72)90020-8

Tschudi, M. A., Meier, W. N., & Scott Stewart, J. (2020). An enhancement to sea ice motion and age products at the National Snow and Ice Data Center (NSIDC). *Cryosphere*, *14*(5). https://doi.org/10.5194/tc-14-1519-2020

Tschudi, M., Meier, W. N., Stewart, J. S., Fowler, C., & Maslanik, J. (2019). EASE-Grid Sea Ice Age, Version 4. In *NASA National Snow and Ice Data Center Distributed Active Archive Center*. https://doi.org/10.5067/UTAV7490FEPB

Tunved, P., & Ström, J. (2019). On the seasonal variation in observed size distributions in northern Europe and their changes with decreasing anthropogenic emissions in Europe: Climatology and trend analysis based on 17 years of data from Aspvreten, Sweden. *Atmospheric Chemistry and Physics*, *19*(23). https://doi.org/10.5194/acp-19-14849-2019

Wang, Q., Jacob, D. J., Fisher, J. A., Mao, J., Leibensperger, E. M., Carouge, C. C., le Sager, P., Kondo, Y., Jimenez, J. L., Cubison, M. J., & Doherty, S. J. (2011). Sources of carbonaceous aerosols and deposited black carbon in the Arctic in winter-spring: Implications for radiative forcing. *Atmospheric Chemistry and Physics*, *11*(23). https://doi.org/10.5194/acp-11-12453-2011

Webster, M. A., Rigor, I. G., Nghiem, S. v., Kurtz, N. T., Farrell, S. L., Perovich, D. K., & Sturm, M. (2014). Interdecadal changes in snow depth on Arctic sea ice. *Journal of Geophysical Research: Oceans*, *119*(8). https://doi.org/10.1002/2014jc009985

Wise, M. E., Baustian, K. J., Koop, T., Freedman, M. A., Jensen, E. J., & Tolbert, M. A. (2012). Depositional ice nucleation onto crystalline hydrated NaCl particles: A new mechanism for ice formation in the troposphere. *Atmospheric Chemistry and Physics*, *12*(2), 1121–1134. https://doi.org/10.5194/acp-12-1121-2012

Yang, X., Frey, M. M., Rhodes, R. H., Norris, S. J., Brooks, I. M., Anderson, P. S., Nishimura, K., Jones, A. E., & Wolff, E. W. (2019). Sea salt aerosol production via sublimating wind-blown saline snow particles over sea ice: Parameterizations and relevant microphysical mechanisms. *Atmospheric Chemistry and Physics*, *19*(13), 8407–8424. https://doi.org/10.5194/acp-19-8407-2019

Yang, X., Neděla, V., Runštuk, J., Ondrušková, G., Krausko, J., Vetráková, L., & Heger, D. (2017). Evaporating brine from frost flowers with electron microscopy and implications for atmospheric chemistry and sea-salt aerosol formation. *Atmospheric Chemistry and Physics*, *17*(10). https://doi.org/10.5194/acp-17-6291-2017

Yang, X., Pyle, J. A., & Cox, R. A. (2008). Sea salt aerosol production and bromine release: Role of snow on sea ice. *Geophysical Research Letters*. https://doi.org/10.1029/2008GL034536

Yang, X., Pyle, J. A., Cox, R. A., Theys, N., & van Roozendael, M. (2010). Snow-sourced bromine and its implications for polar tropospheric ozone. *Atmospheric Chemistry and Physics*, *10*(16), 7763–7773. https://doi.org/10.5194/acp-10-7763-2010

Zhang, L., Gong, S., Padro, J., & Barrie, L. (2001). A size-segregated particle dry deposition scheme for an atmospheric aerosol module. *Atmospheric Environment*, *35*(3). https://doi.org/10.1016/S1352-2310(00)00326-5

Zhou, L., Stroeve, J., Xu, S., Petty, A., Tilling, R., Winstrup, M., Rostosky, P., Lawrence, I. R., Liston, G. E., Ridout, A., Tsamados, M., & Nandan, V. (2021). Inter-comparison of snow depth over Arctic sea ice from reanalysis reconstructions and satellite retrieval. *Cryosphere*, *15*(1). https://doi.org/10.5194/tc-15-345-2021